

PAPER • OPEN ACCESS

Five degrees of freedom test mass readout via optical levers

To cite this article: V Huarcaya *et al* 2020 *Class. Quantum Grav.* **37** 025004

View the [article online](#) for updates and enhancements.






AAS | **IOP Astronomy** ebooks

Part of your publishing universe and your first choice for astronomy, astrophysics, solar physics and planetary science ebooks.

iopscience.org/books/aas

Five degrees of freedom test mass readout via optical levers

V Huarcaya^{1,2}, G Apelbaum^{1,2}, V Haendchen^{1,2}, Q Wang^{1,2,3},
G Heinzl^{1,2} and M Mehmet^{1,2}

¹ Max Planck Institute for Gravitational Physics (Albert Einstein Institute),
Callinstrasse 38, 30167 Hannover, Germany

² Institut für Gravitationsphysik, Leibniz Universität Hannover, Callinstrasse 38,
30167 Hannover, Germany

E-mail: victor.huarcaya@aei.mpg.de and moritz.mehmet@aei.mpg.de

Received 22 October 2019, revised 25 November 2019

Accepted for publication 27 November 2019

Published 19 December 2019



CrossMark

Abstract

High precision measurement of all six degrees of freedom of freely floating test masses is necessary for future gravitational space missions as the sensing noise is frequently a limiting factor in the overall performance of the instrument. Femto-meter sensitivity has been demonstrated with LISA Pathfinder which used a complex laser interferometric setup. However, these measurements were restricted to the length changes in one degree of freedom only. When aiming for sensing multiple degrees of freedom, typically capacitive sensing is used, which facilitates a compact setup but does not provide competitive precision. An alternative approach to improve the sensitivity beyond capacitance readout systems and to reduce the complexity of the setup, is to use optical levers. Here, we report on the realization of a test mass sensing system by means of a modulation/demodulation technique in combination with four optical levers detected by quadrant photodiodes. The results of our table-top experiment show that this configuration allows us to extract information on five degrees of freedom of a cubic test mass. With basic off-the-shelf laser diodes we demonstrate an angular resolution of below $600 \text{ nrad Hz}^{-1/2}$ at frequencies between 10 mHz and 1 Hz (which is better than a conventional autocollimator) while simultaneously measuring the linear motion of the test mass with a precision of better than $300 \text{ nm Hz}^{-1/2}$



Original content from this work may be used under the terms of the [Creative Commons Attribution 3.0 licence](https://creativecommons.org/licenses/by/3.0/). Any further distribution of this work must maintain attribution to the author(s) and the title of the work, journal citation and DOI.

³ Current address: College of Science, Hubei University of Automotive Technology, Shiyan 442002, People's Republic of China

in the same frequency band. Extension of the geometry will enable optical sensing of all six degrees of freedom of the test mass.

Keywords: optical Lever, test mass readout, torsion pendulum, precision measurement

(Some figures may appear in colour only in the online journal)

1. Introduction

Determining and tracking the position of, or the distance between freely floating, macroscopic reference objects, typically test masses (TMs), is the underlying concept for gravity related satellite missions such as LISA (Laser Interferometer Space Antenna) [1] which is planned to be launched around the year 2030 in order to detect gravitational waves. Similarly, GRACE (Gravity Recovery and Climate Experiment, 2002–2017) [2], its follow-on mission GRACE-FO [3, 4], and GOCE (Gravity Field and steady-state Ocean Circulation Explorer, 2009–2013) [5] employ test mass sensing to collect data on the Earth’s gravitational field. The latter three have used capacitive suspension for their accelerometers and gradiometer, respectively, where the science signal is derived from the feedback signal which keeps the TM centered within the inertial sensor by means of capacitive coupling with its specifically designed housing. The technology demonstrator mission LISA Pathfinder [6] (2015–2017) has successfully proven that laser interferometric readout can be used to achieve much higher readout sensitivity. However, the interferometric system implemented therein was limited to sensing one translational and two rotational degrees of freedom (DOFs) and simple upscaling of this technology to achieve readout in 6-DoFs would be challenging in terms of optical complexity and payload dimensions. This has triggered the investigation of novel, more compact concepts such as deep phase modulation interferometry [7] and its variant deep frequency modulation interferometry [8] which both are promising candidates to facilitate high-precision interferometric measurements with a compact optical setup.

Within the framework of developing the gravitational reference sensor (GRS) for LISA-Pathfinder, it has been shown that optical lever arms are a viable option when trying to overcome the limitations due to a capacitive readout scheme [9]. Measurements using a torsion pendulum resulted in a sensitivity of approximately $20 \text{ nrad Hz}^{-1/2}$ at frequencies above 10 mHz obtained with a readout system based on a single optical lever sensed by a quadrant photodiode (QPD), which was about a factor of ten better than the reference sensitivity of the GRS [10]. The system is fairly simple and reliable but allows for exceeding the sensitivity of the capacitive sensor in both translational and rotational DOFs in a wide range of frequencies and improving the sensitivity of the GRS [11, 12]. Optical levers have been widely used for several applications in different science branches, for example, for atomic force microscopy [13], to perform precision angle measurements in combination with interferometry [14] or for adhesion force studies [15]. Albeit not being sensitive enough to achieve the precision of state-of-the-art laser interferometry, its simple optical setup and adaptability to pre-defined geometries make the optical lever a compelling approach especially when aiming for an application where ultra-high precision is not required.

Here we report on the design and test of a readout scheme based on four optical lever arms generated from simple laser diodes reflected off a cubic TM and detected by QPDs. The spatial arrangement of the setup allows for simultaneous sensing of five DoFs of the TM. We employ a hybrid analog and digital modulation-demodulation technique for the measurements

in order to avoid cross-talk between the individual laser beams and the effects of ambient light. A hexapod enabled a dynamic motion and position actuation of the TM. The analysis presented here focuses on the two translational DoFs (TM motion along x and y -axis) and the rotational DoF around the z -axis (θ). To first order, these DoFs contain the information of a TM suspended from a fiber as can be realized in a laboratory setup, for example in a torsion pendulum. In this case, the science signal would be contained in θ while the residual pendulum swing modes could be extracted from the x and y signals. These, in turn can be used to derive a suitable control signal for stabilizing the experimental platform of the torsion pendulum to provide seismic noise isolation. The simultaneous measurement of the remaining rotational DoFs ϕ and ψ (commonly referred to as the pitch and roll angles) provides information on the associated residual cross couplings for all measurements. By additionally measuring the two angular DoFs, θ and ϕ with a commercial autocollimator when a sinusoidal motion is applied to the hexapod, we show that the optical lever performs with a better sensitivity than the commercially available device.

2. Experimental setup

The optical setup is schematically shown in figure 1(a). Four off-the-shelf laser diodes (Thorlabs CPS635R) with an output power of approximately 1 mW at 635 nm in a collimated beam of 2.9 mm diameter, are reflected off four gold-coated mirrors attached to an aluminium cube serving as a mock-up TM. The TM is attached to a hexapod (HXP100-MECA from Newport) which serves as an actuation system for arbitrary movements via its manufacturer-supplied computer interface. Each reflected beam is detected by a silicon QPD with a total active area of 95 mm², split into four quadrants A, B, C, and D. The laser diodes and QPDs are rigidly mounted on a dedicated breadboard, which features a centre hole to fit the hexapod and TM, and was elevated to match the plane of the laser beams with the height of the TM. In this configuration any movement of the TM, except for a translation along the z -axis, results in a simultaneous displacement of the light spot either on two opposing or all QPDs. We developed a USB-interfaced electronics board to drive the laser diodes and to readout the QPDs via a hybrid analog and digital modulation-demodulation scheme. Each laser is intensity modulated at a frequency adjustable via an on-board field-programmable gate array (FPGA) and the frequencies were set to 21, 22, 23, and 24 kHz for LD1 to LD4, respectively. Sixteen trans-impedance amplifiers convert the resulting photo-currents of the quadrants into voltages, where the horizontal and vertical differential voltages for each photo detector are obtained by summing and subtracting circuits which generate $\Delta V_h \propto (A + C) - (B + D)$ and $\Delta V_v \propto (A + B) - (C + D)$. Subsequently, eight analog-to-digital converters (LTC2440) are used to digitize the differential signals. The FPGA is then used to multiply these signals with an electrical copy (local oscillator) of their corresponding modulation frequency to obtain the measurement signals for each QPD. By using differing frequencies and matching local oscillators for each of the four lasers and the respective QPD channel, the measurement signal of one optical lever arm is insensitive to stray light or residual reflections from the other three as well as ambient light. The output of the FPGA is a time-series of the vertical and horizontal signals $\Delta V_{\text{QPD}_{i,v}}$ and $\Delta V_{\text{QPD}_{i,h}}$ ($i = 1, \dots, 4$), respectively, measured with a sampling rate of 1059 Hz and stored as a multi-column ASCII file. As shown below, these output signals contain the information on the TM motion in five degrees of freedom: the translations along the x - and y -axis and the rotation around the z -axis given by θ , plus the rotation on the translational axes given by ϕ and ψ . As can be seen from figure 1, displacing the TM along the x -axis (Δx_{TM}), assuming perfect alignment, does not result in any displacement of the spot on

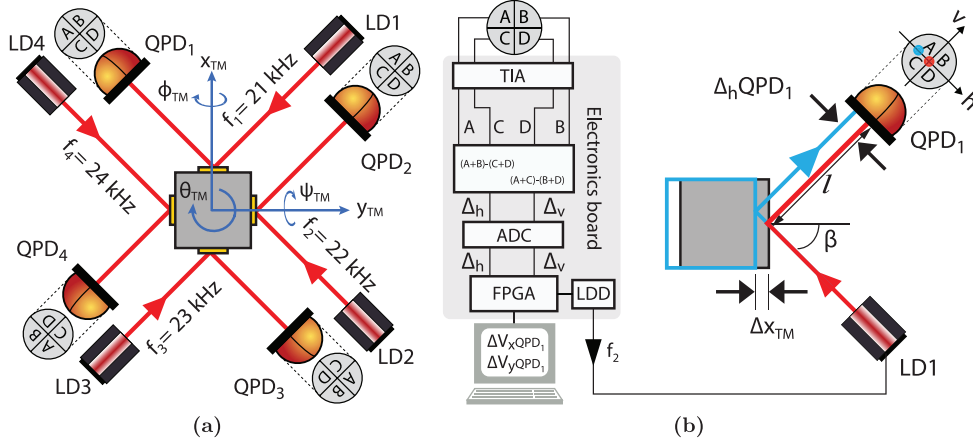


Figure 1. (a) Optical configuration of the experimental setup. Four laser beams from simple laser diodes (LD) are reflected off the test mass mirrors and detected by four quadrant photodetectors (QPDs) with their active area divided into the quadrants A-B-C-D. The lasers are intensity modulated with different modulation frequencies f_1 – f_4 . (b) Geometry of a single optical lever and QPD with corresponding signal processing. A field programmable gate array (FPGA) is used for signal generation and data analysis. This board serves as the laser diode driver (LDD) supplying the modulation frequencies and as the data acquisition system for the QPD signals. For signal analysis, the board comprises a trans-impedance amplifier (TIA) stage followed by amplifier stages to obtain the horizontal and vertical differential voltages Δ_h and Δ_v , which are then digitized by means of analog-to-digital converters (ADC). The digital signals are mixed down and low-pass filtered in the FPGA. The output signals are sent to a computer via USB for real time data display, storage and post processing. In this setup, the total optical lever length l (from QPD to TM mirror) is 225 mm and the angle of incidence $\beta = 45^\circ$. (a) Optical configuration. (b) Data acquisition and geometrical layout.

QPD₂ and QPD₄, but yields a displacement $\Delta_h \text{QPD}$ with opposite sign on the two detectors QPD₁ and QPD₃ that depends on the angle of incidence β ($0 < \beta < \pi/2$), and is given by

$$\Delta_h \text{QPD}_{1,3}(\Delta x_{\text{TM}}) = \pm 2 \sin \beta \cdot \Delta x_{\text{TM}}. \quad (1)$$

The displacement due to a TM rotation $\Delta \theta_{\text{TM}}$ in the x - y -plane is common mode on all detectors and depends on the optical lever length, l , measured from the TM mirror to the QPD:

$$\Delta_h \text{QPD}_{1,2,3,4}(\Delta \theta_{\text{TM}}) = 2l \cdot \Delta \theta_{\text{TM}}, \quad (2)$$

where we have assumed equal lengths for all four optical levers. It is evident from equations (1) and (2) that both motions contribute to the same differential signal, and therefore the total displacement for a TM motion along the x -axis is given by

$$\Delta_h \text{QPD}_{1,3} = \pm 2 \sin \beta \cdot \Delta x_{\text{TM}} + 2l \cdot \Delta \theta_{\text{TM}}, \quad (3)$$

and due to symmetry, QPD₁ and QPD₃ provide a similar expression for the TM motion along the y -axis,

$$\Delta_h \text{QPD}_{2,4} = \pm 2 \sin \beta \cdot \Delta y_{\text{TM}} + 2l \cdot \Delta \theta_{\text{TM}}.$$

The vertical displacements due to pure rotation of the TM around the two remaining angular degrees of freedom ψ (rotation about x -axis) or ϕ (rotation about y -axis) contribute to the signals on two opposing sensors only. Since the laser is not perpendicular to the plane of rotation

for these DoFs, the length of the optical lever scales with the cosine of the angle of incidence, yielding

$$\Delta_v \text{QPD}_{1,3}(\Delta\psi_{\text{TM}}) = \pm 2l \cos \beta \cdot \Delta\psi_{\text{TM}}, \quad (4)$$

and likewise

$$\Delta_v \text{QPD}_{2,4}(\Delta\phi_{\text{TM}}) = \pm 2l \cos \beta \cdot \Delta\phi_{\text{TM}}. \quad (5)$$

Consequently, the output voltages that are generated by our measurement device for any movement of the laser beams across the four QPDs can be described with the following matrix equation:

$$\underbrace{\begin{pmatrix} \Delta V_{\text{QPD}_{1,v}} \\ \Delta V_{\text{QPD}_{1,h}} \\ \Delta V_{\text{QPD}_{2,v}} \\ \Delta V_{\text{QPD}_{2,h}} \\ \Delta V_{\text{QPD}_{3,v}} \\ \Delta V_{\text{QPD}_{3,h}} \\ \Delta V_{\text{QPD}_{4,v}} \\ \Delta V_{\text{QPD}_{4,h}} \end{pmatrix}}_{\Delta \mathbf{V}} = \mathbf{C} \cdot \underbrace{\begin{pmatrix} 0 & 0 & 0 & 2l \cos \beta & 0 \\ 2 \sin \beta & 0 & 2l & 0 & 0 \\ 0 & 0 & 0 & 0 & 2l \cos \beta \\ 0 & 2 \sin \beta & 2l & 0 & 0 \\ 0 & 0 & 0 & -2l \cos \beta & 0 \\ -2 \sin \beta & 0 & 2l & 0 & 0 \\ 0 & 0 & 0 & 0 & -2l \cos \beta \\ 0 & -2 \sin \beta & 2l & 0 & 0 \end{pmatrix}}_{\mathbf{A}} \cdot \underbrace{\begin{pmatrix} \Delta x_{\text{TM}} \\ \Delta y_{\text{TM}} \\ \Delta \theta_{\text{TM}} \\ \Delta \psi_{\text{TM}} \\ \Delta \phi_{\text{TM}} \end{pmatrix}}_{\mathbf{B}}, \quad (6)$$

where $\Delta \mathbf{V}$ comprises the vertical and horizontal output voltage signals, \mathbf{A} is the 5×8 matrix that describes the geometric relationship between the five degrees of freedom of the TM and the eight displacement signals, and the entries of \mathbf{B} are the 5-DoFs of the TM. \mathbf{C} is a diagonal matrix that contains eight calibration factors which comprises four factors ($\mathbf{C}_{i,h}$) for horizontal and four factors ($\mathbf{C}_{i,v}$) for vertical movement of the beam across the active area, respectively, where $i = (1, \dots, 4)$ belong to the respective QPDs used in the setup, $l = 0.225$ m is the optical lever length and $\beta = 45^\circ$ is the angle of incidence.

To derive the TM readout from the raw data given by $\Delta \mathbf{V}$, we compute the inverse matrix $(\mathbf{C} \cdot \mathbf{A})^{-1}$ that links the output signals from the QPDs to the TM displacement. Since $\mathbf{C} \cdot \mathbf{A}$ is not a square matrix, we compute $(\mathbf{C} \cdot \mathbf{A})^{-1}$ by using the left pseudo-inverse matrix $(\mathbf{C} \cdot \mathbf{A})_{\text{left}}^{-1} = ((\mathbf{C} \cdot \mathbf{A})^T (\mathbf{C} \cdot \mathbf{A}))^{-1} (\mathbf{C} \cdot \mathbf{A})^T$. Consequently, the readout of the TM for 5-DoFs can be finally computed as

$$\mathbf{B} = (\mathbf{C} \cdot \mathbf{A})_{\text{left}}^{-1} \cdot \Delta \mathbf{V}. \quad (7)$$

The calibration factors in the matrix \mathbf{C} depend on the shape of the laser beams hitting the sensitive area of the QPDs and the electronic gains of the amplification stages that are used to convert the incident light into differential voltages. \mathbf{C} is diagonal due to the independence of each QPD and since the lasers are different for each QPD, the values $\mathbf{C}_{i,h/v}$ will differ from one to another. To be able to determine the calibration factors and the performance of the optical lever for arbitrary configurations we developed a numerical simulation to predict the response of our system to a motion of the TM. The input to our model were the intensity matrices extracted from images of the laser intensity distributions which were taken with a CMOS beam analyzer camera placed in the respective positions of the four QPDs. As an example, the simulated differential power signal on QPD2 due to the TM moving along the x -axis is plotted in figure 2. The inset shows the corresponding camera image of the beam impinging onto QPD2.

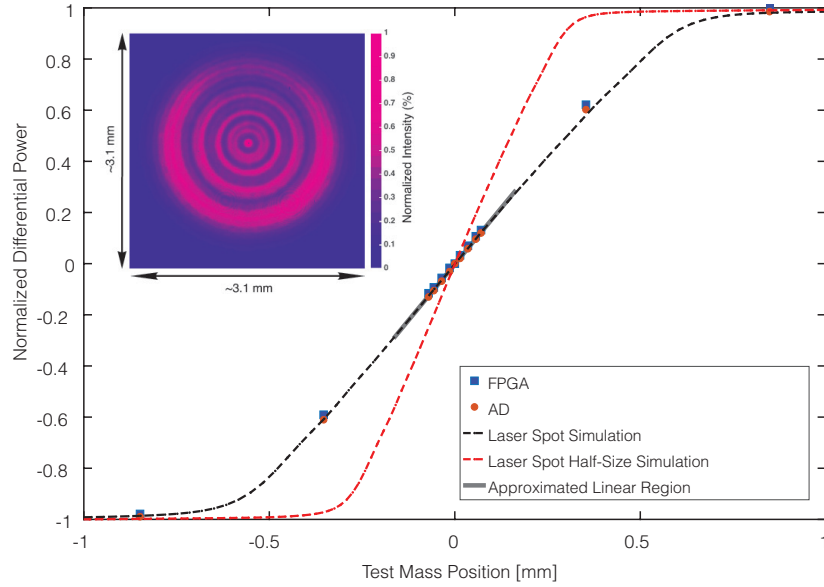


Figure 2. Differential output signal from QPD2 due to TM motion along x -axis. The dashed black line is a simulation with the numerical model based on the intensity image of the beam impinging on QPD2. The corresponding camera image is shown in the inset. The circular ring pattern is caused by diffraction at the laser diode apertures. From an estimate of the linear region (thick gray line) we can deduce the calibration factor via the geometrical properties of the optical lever. The dashed red line shows a simulation of the system response for a laser spot with half the diameter. The blue squares and red dots are signals measured with our system and an independent conventional analog readout circuit, respectively.

From the analytical model we can deduce how a change of the geometry and/or the beam shape will affect our measurements, as for example, a smaller laser spot will reduce the dynamical range, while the slope and hence the sensitivity will increase equally for sensing Δx_{TM} , Δy_{TM} and $\Delta \theta_{\text{TM}}$. From our model, the values of the calibrations factors $C_{i,h/v}$ can be obtained by estimating the linear slope for $\Delta x \approx 0$ due to a horizontal beam displacement. In order to verify the results, we performed a direct calibration for each QPD. To this end, we measured the response to horizontal beam displacement by mounting each QPD on a micrometer translation stage. The voltage signal was recorded as a function of the displacement perpendicular to the incident laser beam. Subsequently the slopes or calibration factors, $C_{i,h}$, were obtained by a linear regression. The good agreement between simulation and the directly measured calibrations factors allows us to predict the corresponding factors for a vertical beam displacement, which are required for extraction of the rotation angles ψ_{TM} and ϕ_{TM} . The QPDs readout voltages can be normalized with respect to the maximum voltage which is found by pointing the laser spot onto one half of the respective QPD. This voltage is then used as a dividing factor for all measurements. As long as the laser spot is inside the QPD the normalized readout values $\Delta V_{\text{N,QPD}_i}$ are between $[-1, 1]$. By assuming linearity and small displacements we obtain a full model for the vertical and horizontal QPD signals. The results of both experimental and computational values and their deviation are shown in table 1.

Table 1. Normalised calibration factors $\mathbf{C}_{i,h,v}$. Values $\mathbf{C}_{i,h}$ were measured for each QPD and compared to the corresponding values obtained from the simulation. The average deviation is around 2%. Since the standard deviation was below 1% it was omitted in this table. The factors for vertical beam displacement $\mathbf{C}_{i,v}$ were derived from the simulation only.

Calibration Factors	QPD1 (m^{-1})	QPD2 (m^{-1})	QPD3 (m^{-1})	QPD4 (m^{-1})
Experimental $\mathbf{C}_{i,h}$	943.4	878.1	874.4	858.2
Simulation $\mathbf{C}_{i,h}$	983.3	894.4	878.1	873.6
Deviation (%)	4.2	1.8	0.4	1.8
Simulation $\mathbf{C}_{i,v}$	1052.4	1025.4	1059	1141.3

3. TM motion sensing

In order to test the system response to a dynamic TM motion we used the hexapod as an actuation stage. Different control programs were developed that allow the motion of the TM in x , y and θ . Independent measurements were taken for the three types of hexapod motion. The resulting time series for the derived TM motion in five DoFs are plotted in figure 3. The longitudinal displacements along x and y are given in μm and the rotation around the 3 axis are given in mrad. For the two translational degrees of freedom the hexapod performed a motion from 0 to $-300 \mu\text{m}$ and to $+300 \mu\text{m}$, respectively. For the angular displacement, i.e. rotation around its vertical symmetry axis, the hexapod was programmed to perform a quasi-sinusoidal motion with an amplitude of ± 1.05 mrad and period of ~ 12.6 min. As expected, the derived signals for the associated intended motion (blue traces) are the most dominant ones for each column. For perfect symmetry, all remain signals should be zero. However, due to imperfections of the setup, for every motion we find cross couplings (red traces) to the other degrees of freedom. For example, the cross coupling between x - and y motion can be explained by an angular mismatch of the TM coordinate system with respect to the hexapod basis. A deviation of only $5 \mu\text{rad}$ accounts for the observed coupling coefficient of $1/200$ ($3 \mu\text{m}$ cross-coupling due to $600 \mu\text{m}$ TM translation). The coupling of translation into the rotational degrees of freedom can be caused by non-parallel mirror surfaces which is likely due to the limited accuracy of the mechanical construction. The cross coupling for a hexapod rotation (right column) can be the result of a tilt and/or displacement mismatch between the z -axis of TM and hexapod. Furthermore, the cross couplings also show a non-negligible hysteresis of the hexapod as the start and stop position for every motion were programmed to be the same, but the corresponding signals do not always match. The three main degrees of freedom analyzed above, were chosen because to first order, these describe the motion of a TM suspended from a thin fiber as it is the case in a torsion balance and the first application of our device will be to sense the corresponding motion in order to control and stabilize its operating point. Sensing the associated pendulum swing modes requires knowledge about the TM translation while the science signal is contained in the rotation. By disentangling rotation from translation, we plan to extract a suitable feedback signal to counteract the unwanted swing modes which are excited, for example, by the seismic coupling into the measurement band. The signals for the remaining two degrees of freedom, ψ_{TM} and ϕ_{TM} , will aid to mitigate cross-couplings and misalignments in a future setup. Later on, these signals will be helpful to study the behaviour of the torsion balance under operation.

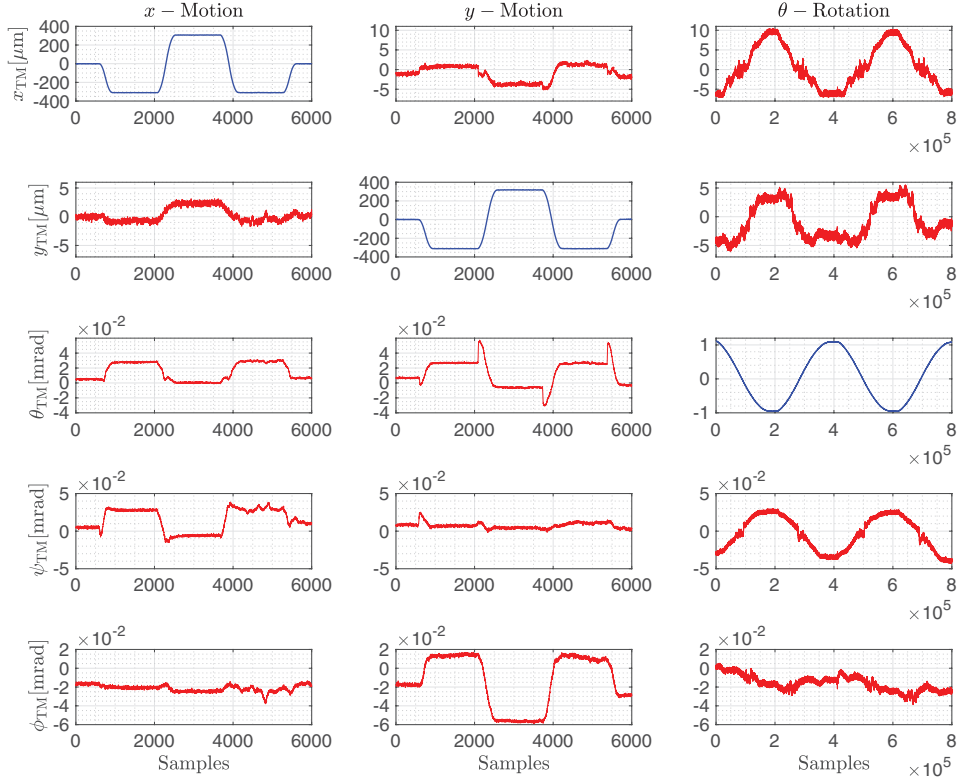


Figure 3. Analysis of five degrees of freedom of the TM. The signals in x_{TM} , y_{TM} , θ_{TM} , ψ_{TM} , and ϕ_{TM} as measured by the optical lever are plotted as a time series recorded with a sampling rate of 1059 Hz. Left column: data for x -motion of the hexapod. Centre column: data for y -motion of the hexapod. The range of motion was $\mp 300 \mu\text{m}$, where the TM translation was programmed to start from zero and return to zero after passing the minimum (maximum) twice (once). Right column: readout data for a test mass rotation around its vertical symmetry axis. A quasi-sinusoidal motion of two cycles with an amplitude of $\sim \pm 1.05 \text{ mrad}$ and period of $\sim 12.6 \text{ min.}$ was applied to the hexapod. While the intended motions (blue traces) are clearly the most prominent signal, the analysis also reveals cross couplings in the other degrees of freedom (red traces).

3.1. Performance and sensitivity

To investigate the performance of our system we conducted a simultaneous measurement of the TM motion θ_{TM} and ϕ_{TM} with our optical levers and an autocollimator (Trioptics TA 100-38). The autocollimator measures small angular displacements by measuring the angle between its own transmitted and received collimated beam of light and is a standard tool to determine small angular displacements, for example, to align components in an optical setup and to detect tiny rotations of a reflecting surface such as a laser mirror. These devices are typically used to sense the rotation in torsion pendulum experiments [16]. The measurements are shown in figure 4, for which we performed five cycles of a sinusoidal TM motion with an amplitude of $\sim 0.5 \text{ mrad}$ and period of $\sim 12.6 \text{ min.}$ The sampling frequency of the acquisition was 1059 Hz for the optical lever and 44.5 Hz for the autocollimator acquisition. The readout of the TM rotation angle θ_{TM} , which is the nominal motion in this measurement, is plotted in figure 4(a). We observed a good agreement between both data sets. The difference

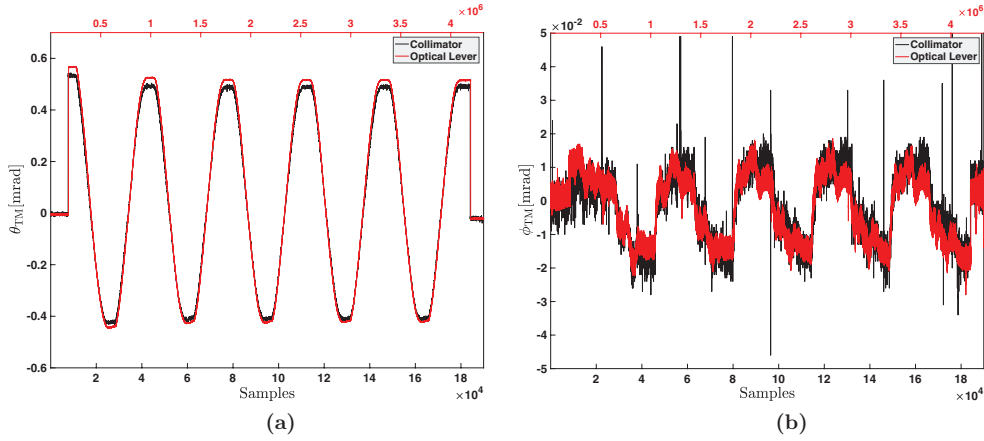


Figure 4. Readout of θ_{TM} and ϕ_{TM} as measured by the optical lever and autocollimator simultaneously for five cycles of a sinusoidal motion with an amplitude of ± 0.5 mrad and a period of ~ 12.5 min. The sharp peaks were caused by electronic pick-up. (a) Readout of the angle θ measured simultaneously with the optical lever and autocollimator. (b) Simultaneous readout of the associated cross-coupling into the angle ϕ .

in amplitude is probably caused by the misalignments present in the setup. The associated cross-coupling into ϕ_{TM} is shown in figure 4(b). We find a discrepancy between the two measurement methods of the order of $1 \mu\text{rad}$. This is close to the resolution limit of the autocollimator, which according to the technical data provided by the manufacturer has a resolution of around $0.5 \mu\text{rad}$ and an accuracy of $12.5 \mu\text{rad}$. The sharp peaks present in the collimator data are measurement artifacts, probably caused by electronic pick-up, and do not represent measurements values.

Figure 5 displays spectral densities of the angular sensitivity obtained from the measured time series via a Fourier transform algorithm [17, 18]. In figure 5(a) we have plotted as trace (a) the spectral density of the electronic dark noise of our apparatus measured while in operation but with all laser diodes blocked such that no light was reaching the photo detectors. This trace lies at a level of around $50 \text{ nrad Hz}^{-1/2}$ which, for the given setup, sets a lower limit to the achievable sensitivity level. Trace (b) is the noise performance with all four optical levers active but without any intentional movement of the hexapod and trace (c) shows the equivalent measurement done with the autocollimator. These steady state sensitivities are about $3.3 \times 10^{-7} \text{ rad Hz}^{-1/2}$ at 100 mHz for the optical lever and $4.2 \times 10^{-6} \text{ rad Hz}^{-1/2}$ for the autocollimator, respectively. In the frequency band from 10 mHz to approximately 2 Hz the minimum resolvable rotational motion obtained with our optical lever system is about one order of magnitude below the autocollimator sensitivity. The same analysis as for trace (a) and (b) was performed for the translational degrees of freedom (figure not shown) which yielded a steady state sensitivity of approximately $200 \text{ nm Hz}^{-1/2}$ at 100 mHz with the electronic dark noise limit at the level of $20 \text{ nm Hz}^{-1/2}$. To estimate and compare the two independent measurement methods we used the same rotational hexapod motion as for the time series presented in figure 4(a). The noise performances obtained with this sinusoidal motion are shown in figure 5(b). Both the optical lever and the autocollimator measurements, plotted in trace (d) and (e), respectively, yield the same signal signature correctly recovering the driving frequency of 1.3 mHz. However, at frequencies above approximately 60 mHz the lower noise floor of the optical lever system allows for a significantly better performance than the autocollimator. This even enables the recovery of the harmonic peaks due the discontinuous nature of the

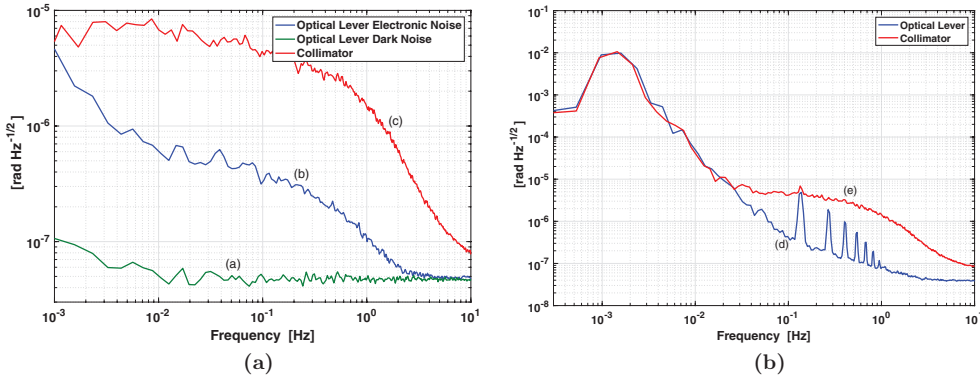


Figure 5. Left: trace (a) shows the electronic dark noise of the optical lever system. The steady state performance of the optical lever and the autocollimator are shown in trace (b) and (c), respectively. Right: comparison between the optical lever and autocollimator angular signal derived from five cycles of a sinusoidal motion with an amplitude of ± 0.5 mrad and period of ~ 12.6 min. (a) Electronic dark noise of the optical lever and steady state performances of autocollimator and optical lever measurements. (b) Measured angular noise of the optical lever and autocollimator for continuous rotation of the TM around the vertical symmetry axis.

hexapod motion. The entire setup had neither seismic nor acoustic isolation and the tests were performed without considering beam jitters, current noise and other external noise sources such as mechanical vibrations, air currents, or temperature variations causing thermal drifts. By introducing proper mitigation strategies the large difference between trace (a) and (b) can most likely be decreased to improve the sensitivity even further.

4. Conclusion

We have presented an optical test mass readout system based on the combination of four optical levers and quadrant photodiodes. Our systems allows for an independent measurement of the five degrees of freedom x_{TM} , y_{TM} , θ_{TM} , ψ_{TM} , and ϕ_{TM} of a cubic test mass. We have shown that these can be measured simultaneously and that our signal analysis allowed us to disentangle TM rotations and translations. This feature was used to reveal cross couplings due non-perfect alignment of the setup and the hysteresis introduced by the hexapod. Albeit being a simple and economic device built from off-the-shelf laser diodes and QPDs, we were able to demonstrate an angular and translational resolution below $600 \text{ nrad Hz}^{-1/2}$ and $300 \text{ nm Hz}^{-1/2}$, respectively, at frequencies between 10 mHz and 1 Hz. We compared the rotational sensing performance against a commercial autocollimator. The angular displacement spectral density yielded a sensitivity of $330 \text{ nrad Hz}^{-1/2}$ at 100 mHz which was about an order of magnitude below the simultaneously recorded data from the autocollimator (about $4.2 \mu\text{rad Hz}^{-1/2}$). Furthermore, the better signal-to-noise ratio enabled signal analysis at frequencies above 100 mHz revealing the higher harmonic peaks due to the discontinuous motion of the hexapod. The first application of our sensor system will be to distinguish between the rotational and swing modes of a torsion pendulum in order to extract a suitable feedback signal for stabilization of the operating point. Since this system will operate under high vacuum, we expect an even better sensitivity as noise sources such as temperature fluctuation, air flow, and acoustic coupling will be smaller. In future the geometry could be

extended by an additional optical lever which senses the vertical motion of the TM to realize an all optical 6 degree of freedom TM sensor.

Acknowledgments

The authors would like to thank the DFG Sonderforschungsbereich (SFB) 1128 Relativistic Geodesy and Gravimetry with Quantum Sensors (geo-Q) for financial support. This work has been supported by the Chinese Academy of Sciences (CAS) and the Max Planck Society (MPG) in the framework of the LEGACY cooperation on low-frequency gravitational wave astronomy (M.IF.A.QOP18098).

ORCID iDs

V Huarcaya  <https://orcid.org/0000-0002-5024-720X>

G Heinzel  <https://orcid.org/0000-0003-1661-7868>

M Mehmet  <https://orcid.org/0000-0001-9432-7108>

References

- [1] Amaro-Seoane P *et al* 2017 (arXiv:1702.00786)
- [2] Tapley B, Bettadpur S, Watkins M and Reigber C 2004 *Geophys. Res. Lett.* **31** 4
- [3] Flechtner F, Morton P, Watkins M and Webb F 2014 Status of the grace follow-on mission *Gravity, Geoid and Height Systems* ed U Marti (Cham: Springer) pp 117–21
- [4] Abich K *et al* 2019 *Phys. Rev. Lett.* **123** 031101
- [5] Drinkwater M R, Floberghagen R, Haagmans R, Muzi D and Popescu A 2003 *GOCE: ESA's First Earth Explorer Core Mission* (Dordrecht: Springer) pp 419–32
- [6] Zononi C, Bortoluzzi D, Conklin J W, Köker I, Seutchat B and Vitale S 2015 *J. Phys.: Conf. Ser.* **610** 012022
- [7] Heinzel G, Cervantes F G, Marín A F G, Kullmann J, Feng W and Danzmann K 2010 *Opt. Express* **18** 19076–86
- [8] Isleif K S, Gerberding O, Schwarze T S, Mehmet M, Heinzel G and Cervantes F G 2016 *Opt. Express* **24** 1676–84
- [9] Acernese F, Calloni E, Rosa R D, Fiore L D, Garcia L and Milano L 2004 *Class. Quantum Grav.* **21** S621–7
- [10] Cavalleri A *et al* 2009 *J. Phys.: Conf. Ser.* **154** 012012
- [11] Acernese F, De Rosa R, Di Fiore L, Garufi F, La Rana A and Milano L 2006 *AIP Conf. Proc.* **873** 339–43
- [12] Grado A, Rosa R D, Fiore L D, Garufi F, Milano L, Russano G and Spagnuolo V 2017 *J. Phys.: Conf. Ser.* **840** 012047
- [13] Meyer G and Amer N M 1988 *Appl. Phys. Lett.* **53** 1045–7
- [14] Hogan J M, Hammer J, Chiow S W, Dickerson S, Johnson D M S, Kovachy T, Sugarbaker A and Kasevich M A 2011 *Opt. Lett.* **36** 1698–700
- [15] Panduputra Y, Ng T W, Neild A and Ling W Y L 2011 *Opt. Lett.* **36** 175–7
- [16] Bassan M *et al* 2016 *Phys. Rev. Lett.* **116** 051104
- [17] Trobs M and Heinzel G 2006 *Measurement* **39** 120–9
- [18] Trobs M and Heinzel G 2009 *Measurement* **42** 170–0